

AD-A219 500

# Atomic Velocity Distributions Out of Hydrogen Maser Dissociators

B. JADUSZLIWER and Y. C. CHAN  
Chemistry and Physics Laboratory  
Laboratory Operations  
The Aerospace Corporation  
El Segundo, CA 90245

15 February 1990

Prepared for  
SPACE SYSTEMS DIVISION  
AIR FORCE SYSTEMS COMMAND  
Los Angeles Air Force Base  
P.O. Box 92960  
Los Angeles, CA 90009-2960

RECEIVED  
FEB 15 1990  
D

APPROVED FOR PUBLIC RELEASE;  
DISTRIBUTION UNLIMITED

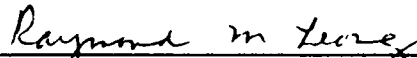
This report was submitted by The Aerospace Corporation, El Segundo, CA 90245, under Contract No. F04701-88-C-0089 with the Space Systems Division, P.O. Box 92960, Los Angeles, CA 90009-2960. It was reviewed and approved for The Aerospace Corporation by J. M. Straus, Director, Chemistry and Physics Laboratory. Lt Cynthia Beagle was the project officer for the Mission-Oriented Investigation and Experimentation (MOIE) Program.

This report has been reviewed by the Public Affairs Office (PAS) and is releasable to the National Technical Information Service (NTIS). At NTIS, it will be available to the general public, including foreign nationals.

This technical report has been reviewed and is approved for publication. Publication of this report does not constitute Air Force approval of the report's findings or conclusions. It is published only for the exchange and stimulation of ideas.



CYNTHIA BEAGLE, LT, USAF  
MOIE Program Officer  
SSD/CWNZS



RAYMOND M. LEONG, MAJ, USAF  
MOIE Program Manager  
AFSTC/WCO OL-AB

UNCLASSIFIED

SECURITY CLASSIFICATION OF THIS PAGE

## REPORT DOCUMENTATION PAGE

1a. REPORT SECURITY CLASSIFICATION Unclassified			1b. RESTRICTIVE MARKINGS		
2a. SECURITY CLASSIFICATION AUTHORITY			3. DISTRIBUTION/AVAILABILITY OF REPORT		
2b. DECLASSIFICATION/DOWNGRADING SCHEDULE			Approved for public release; distribution unlimited.		
4. PERFORMING ORGANIZATION REPORT NUMBER(S) TR-0090(5945-05)-1			5. MONITORING ORGANIZATION REPORT NUMBER(S) SSD-TR-90-02		
6a. NAME OF PERFORMING ORGANIZATION The Aerospace Corporation Laboratory Operations		6b. OFFICE SYMBOL (If applicable)	7a. NAME OF MONITORING ORGANIZATION Space Systems Division		
6c. ADDRESS (City, State, and ZIP Code) El Segundo, CA 90245-4691		7b. ADDRESS (City, State, and ZIP Code) Los Angeles Air Force Base Los Angeles, CA 90009-2960			
8a. NAME OF FUNDING/SPONSORING ORGANIZATION		8b. OFFICE SYMBOL (If applicable)	9. PROCUREMENT INSTRUMENT IDENTIFICATION NUMBER F04701-88-C-0089		
8c. ADDRESS (City, State, and ZIP Code)		10. SOURCE OF FUNDING NUMBERS			
		PROGRAM ELEMENT NO.	PROJECT NO.	TASK NO.	WORK UNIT ACCESSION NO.
11. TITLE (Include Security Classification) Atomic Velocity Distributions Out of Hydrogen Maser Dissociators					
12. PERSONAL AUTHOR(S) Jaduszliwer, B.; and Chan, Y. C.					
13a. TYPE OF REPORT		13b. TIME COVERED FROM _____ TO _____		14. DATE OF REPORT (Year, Month, Day) 15 February 1990	
				15. PAGE COUNT 29	
16. SUPPLEMENTARY NOTATION.					
17. COSATI CODES			18. SUBJECT TERMS (Continue on reverse if necessary and identify by block number)		
FIELD	GROUP	SUB-GROUP	Atomic clocks; Hydrogen maser; Hydrogen dissociator; Velocity distributions.		
19. ABSTRACT (Continue on reverse if necessary and identify by block number) <i>are determined for</i> We have determined velocity distributions of atoms effusing out of radio frequency discharge hydrogen dissociators, of the type used in hydrogen masers. This work was motivated by long-term reliability issues related to the possible use of masers as frequency standards on satellites. A primary issue is the maser's hydrogen budget, because many of the common failure modes of a maser involve either the hydrogen source or sink. Because the focusing properties of the state-selecting magnets are velocity dependent, the overall hydrogen budget will depend not only on the dissociation efficiency but also on the velocity distribution of the hydrogen atoms leaving the dissociation. Many times, that distribution has been tacitly assumed to be Maxwellian at wall temperature, but that assumption is not necessarily valid. Our measurements show the distributions to be much narrower than Maxwellian and to broaden as the hydrogen pressure in the dissociator increases. Operating the dissociator to yield a relatively narrow velocity distribution and using a state-selecting magnet well matched to that distribution may significantly improve the efficiency of hydrogen use by the maser. <i>See words.</i>					
20. DISTRIBUTION/AVAILABILITY OF ABSTRACT <input type="checkbox"/> UNCLASSIFIED/UNLIMITED <input checked="" type="checkbox"/> SAME AS RPT. <input type="checkbox"/> DTIC USERS			21. ABSTRACT SECURITY CLASSIFICATION Unclassified		
22a. NAME OF RESPONSIBLE INDIVIDUAL			22b. TELEPHONE (Include Area Code)		22c. OFFICE SYMBOL

# CONTENTS

I.	INTRODUCTION.....	5
II.	EXPERIMENTAL APPARATUS.....	7
III.	ATOMIC DEFLECTION IN A "TWO-WIRE" MAGNETIC FIELD.....	9
IV.	CALIBRATION AND PROOF-OF-CONCEPT EXPERIMENT.....	13
V.	ATOMIC HYDROGEN VELOCITY DISTRIBUTIONS.....	17
VI.	DISCUSSION AND CONCLUSIONS.....	25
	REFERENCES.....	29

Accession For	
NTIS GPO/CI	<input checked="" type="checkbox"/>
DTIC TAB	<input type="checkbox"/>
Unannounced	<input type="checkbox"/>
Justification	
By	
Distribution/	
Availability Codes	
Dist	Avail and/or Special
A-1	



## FIGURES

1.	Schematic View of the Experimental Arrangement.....	8
2.	Cross Section of the "Two-Wire" Field Magnet.....	10
3.	Rubidium Atomic Beam Signal (Detector and Oven on Axis) vs Magnet Coil Current.....	14
4.	Detected Rubidium Atom Distributions at Indicated Magnetic Fields.....	16
5.	Atomic Hydrogen Beam Fraction vs rf Discharge Power.....	18
6.	Detected Hydrogen Atom Distribution at 995 G and 0.40 Torr.....	19
7.	Detected Hydrogen Atom Distribution at 995 G and 0.20 Torr.....	21
8.	Detected Hydrogen Atom Distribution at 995 G and 0.40 Torr.....	22
9.	Detected Hydrogen Atom Distribution at 995 G and 0.70 Torr.....	23
10.	Model Velocity Distributions Used for Fig. 7.....	26
11.	Model Velocity Distributions Used for Fig. 8.....	27
12.	Model Velocity Distributions Used for Fig. 9.....	28

## I. INTRODUCTION

The use of hydrogen masers as frequency standards on spacecraft requires careful consideration of long-term reliability issues. A primary issue is the maser's hydrogen budget, because many of the common failure modes of a hydrogen maser involve either the hydrogen source (storage or dissociator) or sink (ion pump or getters). An excess of hydrogen atoms in the  $F = 1$ ,  $M = 0$  state must be continuously fed into the maser bulb. The ratio of the rates at which atoms in the proper hyperfine state enter the bulb and molecules are fed into the dissociator will impact strongly the maser's long-term reliability. This ratio will be determined mainly by the dissociator's efficiency and the properties of the state-selecting magnet. Atomic state selection is performed in hydrogen masers by a quadrupole or hexapole magnet, which focuses atoms in the  $F = 1$ ,  $M = 0$  state at the bulb's entrance orifice and defocuses the  $F = 0$ ,  $M = 0$  atoms. The focal length of those magnets depends strongly on atomic speed, and typically only a narrow range of atomic velocities will be focused. Clearly, dissociators yielding narrower velocity distributions could more efficiently use the hydrogen supply.

Relatively little is known of the velocity distribution of atoms effusing out of radio frequency (rf) discharge hydrogen dissociators. In many cases, the tacit assumption is made that the atoms will be in thermal equilibrium with the dissociator wall, but that is not necessarily true. The threshold for molecular dissociation by collisions with discharge electrons is about 8.5 eV. Because the molecular binding energy is approximately 4.7 eV, each atom carries away an excess energy of about 2 eV (Ref. 1). Depending on dissociator geometry and gas density, the hydrogen atoms may or may not undergo enough gas and wall collisions to thermalize fully. Walraven and Silvera (Ref. 2) have studied the characteristics of a beam of hydrogen atoms produced in a microwave discharge followed by a thermal accommodator and found the velocity distributions to be Maxwellian at the accommodator temperature. Hershcovitch et al. (Ref. 3) studied a similar dissociator-and-accommodator

combination, operated at higher pressures and flow rates, and measured velocity distributions in reasonable agreement with the calculated supersonic-flow distributions. Because thermal accommodators are not commonly used in maser dissociators, these results are not directly applicable to our problem. Miller (Ref. 4) investigated a helium-cooled microwave discharge dissociator at relatively high pressure (3.3 Torr) and measured a velocity distribution that was slightly narrower than the Maxwellian at the estimated discharge temperature. We are studying the velocity distributions of atomic hydrogen produced in an rf discharge dissociator having a geometry and operating parameters resembling those of a maser dissociator. The experimental technique and preliminary results are presented in this report.

## II. EXPERIMENTAL APPARATUS

Atomic hydrogen velocity distributions have been determined using a magnetic deflection technique. Figure 1 exhibits the experimental arrangement. Hydrogen is fed through a standard, temperature-controlled Pd-Ag alloy leak (Ref. 5) into a cylindrical, double-walled Pyrex bulb. The bulb is 15 cm long, with a 1.9 cm internal diameter and a 3.8 cm external diameter. Compressed air flows between the walls to provide cooling, and rf power is inductively coupled to the discharge through an external 25-turn coil. The hydrogen beam exits the dissociator through a slit that is 0.1 cm long and 0.025 cm wide, and is collimated by a second slit that is 0.025 cm wide, set at  $d = 63.7$  cm away from the source slit. The beam then travels between the pole pieces of an  $L = 11.4$  cm long electromagnet configured in the "two-wire" geometry described by Rabi et al. (Ref. 6). After additional travel through a drift tube that is  $D = 71.3$  cm long, the beam is detected by a quadrupole mass analyzer.

Molecular hydrogen, having no magnetic dipole moment, will travel through the magnet without deflection, but the hydrogen atoms will be deflected by the inhomogeneous magnetic field. The dissociator is attached to the rest of the apparatus by flexible vacuum bellows and can be displaced transversally by micrometer screws. In this way, the angular distribution of atoms deflected by the field can be measured.



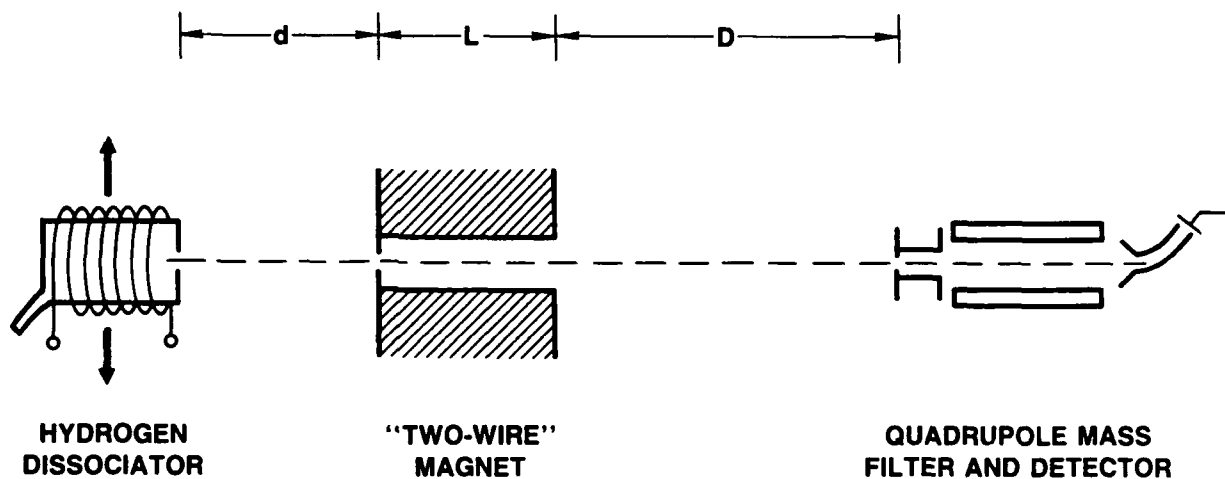


Fig. 1. Schematic View of the Experimental Arrangement.  
The hydrogen dissociator can be displaced transversally.

### III. ATOMIC DEFLECTION IN A "TWO-WIRE" MAGNETIC FIELD

An atom having magnetic moment  $\vec{\mu}$ , immersed in a magnetic field  $\vec{H}$ , has an energy  $E = -\vec{\mu} \cdot \vec{H}$ . The force acting on the atom is  $\vec{F} = -\text{grad}(\vec{\mu} \cdot \vec{H}) \approx \mu_{\text{eff}} \text{grad}(H)$ , where  $\mu_{\text{eff}}$  is the component of the atomic magnetic moment along the field direction. In general,  $\mu_{\text{eff}}$  will depend on the atomic ground state quantum numbers and the magnetic field strength. If an atom has total electron angular momentum  $J = 1/2$  and nuclear spin  $I$ , both in units of  $\hbar/2\pi$ , then its effective magnetic moment is given by Breit-Rabi's formula (Ref. 7)

$$\mu_{\text{eff}} = \pm \frac{\epsilon + 2M/(2I + 1)}{[1 + 4M\epsilon/(2I + 1) + \epsilon^2]^{1/2}} \mu_0 \quad (1)$$

where the "+" sign corresponds to total angular momentum  $F = I - 1/2$ , the "-" sign to  $F = I + 1/2$ , and  $M$  is the total azimuthal quantum number.  $\epsilon$  is proportional to the ratio of magnetic-to-hyperfine energy,  $\epsilon = g_L \mu_0 H/W$ , where  $g$  is the Lande factor for the atom,  $\mu_0$  is the Bohr magneton, and  $W$  is the atomic hyperfine splitting.

Figure 2 exhibits the cross section of the "two-wire" magnet;  $2\alpha$  is the separation between the "equivalent wires" (Ref. 8). If a narrow atomic beam enters the magnet at  $x = 1.2\alpha$  (as determined by the collimating slit) and the atomic transversal displacements within the magnet are small, then the force acting on the atoms remains approximately constant (Ref. 9), and so does the acceleration:

$$a \approx \frac{0.984}{\alpha} \frac{\mu_{\text{eff}}}{m} H \hat{i} \quad (2)$$

where  $H$  is the magnetic field intensity at the atomic beam,  $m$  is the atomic mass, and  $\hat{i}$  is a unit vector pointing along the  $x$  axis. Under these conditions, the trajectory equations for the atoms traveling from source to detector can be solved easily. With no magnetic field, an atom of magnetic moment  $\mu_{\text{eff}}$  and speed  $V$  leaving the source slit at  $x_S$  will be detected at  $x_D = -x_S (L + D)/d$ . If the magnetic field is set at  $H$  and the detector is not

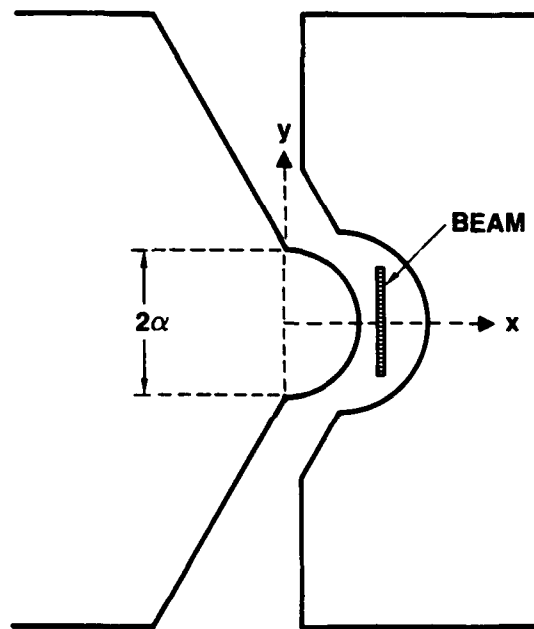


Fig. 2. Cross Section of the "Two-Wire" Field Magnet.  
 $2\alpha$  is the separation of the "equivalent wires."

moved, an identical atom will have to leave the plane of the source slit at  $x_S'$ , given by

$$x_S' \approx x_S + \frac{a}{v^2} \frac{Ld}{2} \left(1 + \frac{D}{L+D}\right) \quad (3)$$

in order to be detected. If  $f_0(x_S)$  is the distribution of detected atoms as a function of source slit position at zero magnetic field, and  $g(V)$  is the speed distribution of atoms leaving the source slit, then the distribution of detected atoms at nonzero field,  $f(x_S)$ , will be given by

$$f(x_S) \approx \sum_{F,M} \int_0^{\infty} f_0(x_S - K_{FM}/V^2) g(V) dV \quad (4)$$

where

$$K_{FM} = \frac{0.492}{\alpha} \frac{\mu_{eff}}{m} H Ld \left(1 + \frac{D}{L+D}\right) \quad (5)$$

Both  $f_0(x_S)$  and  $f(x_S)$  can be measured, and then Eq. (4) can be used to verify whether a given velocity distribution is consistent with these measured distributions.

#### IV. CALIBRATION AND PROOF-OF-CONCEPT EXPERIMENT

A preliminary experiment to study the deflection of a rubidium beam was performed to calibrate the electromagnet and test the use of Eq. (4) to verify an assumed velocity distribution.

Equation (1) reveals that for an atom having nuclear spin  $I$ ,  $\mu_{\text{eff}} = 0$  if  $\epsilon = -2M/(2I + 1)$ . At field intensities determined by

$$H = \frac{-M}{2I + 1} \frac{W}{\mu_0} \quad (6)$$

atoms with  $M < 0$  will not be deflected by the field. Natural rubidium is a mixture of 72.2%  $\text{Rb}_{85}$  ( $I = 5/2$ ) and 27.8%  $\text{Rb}_{87}$  ( $I = 3/2$ ).  $\text{Rb}_{85}$  will have zero effective moments at  $H = 361$  G ( $M = -1$ ) and  $H = 722$  G ( $M = -2$ ).  $\text{Rb}_{87}$  will have a zero effective moment at  $H = 1221$  G ( $M = -1$ ). Figure 3 exhibits the detected atomic signal as a function of magnet coil current, with the rubidium beam source and detector on the apparatus axis. At the field values just listed, atoms in the zero effective moment states will travel through the magnet without deflection, leading to an increased signal. The effect of the zero effective moment states can be made more apparent on the figure by subtracting the local sloping background from each one of the marked features. The peaks labeled A and B can then be identified with the zero effective moments at 722 and 1221 G, respectively, yielding a calibration of 66.3 G/A for the magnet.

The rubidium source for these measurements was a two-chambered oven designed and operated to ensure effusive flow. Under those conditions, the atomic beam speed distribution should be beam-Maxwellian:

$$g(V) = (2/\beta) (V/\beta)^3 \exp [-(V/\beta)^2] \quad (7)$$

where  $\beta = \sqrt{(2kT/m)}$  and  $T$  is the oven temperature. We measured  $f(x_S)$  for  $H = 1061$  G,  $H = 1220$  G, and  $H = 1525$  G, and also measured  $f_0(x_S)$ . We then used Eq. (4), with the speed distribution given by Eq. (7), to calculate the

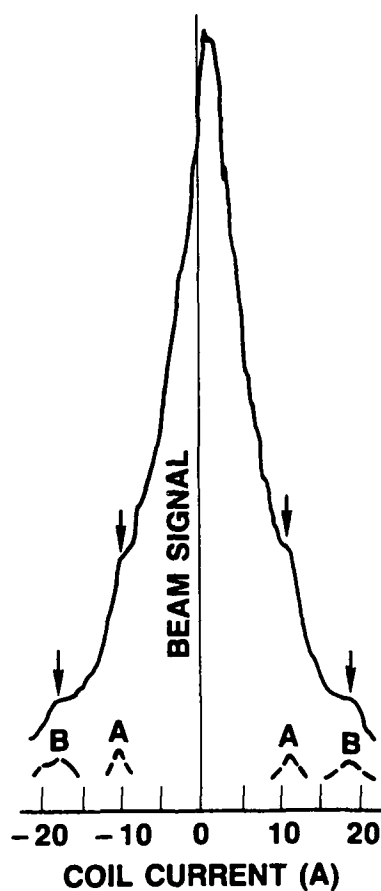


Fig. 3. Rubidium Atomic Beam Signal (Detector and Oven on Axis) vs Magnet Coil Current. Arrows exhibit features resulting from zero effective moment states. Dashed lines were obtained by subtracting the local constant-slope background from each feature. A:  $\text{Rb}_{85}$ ,  $M = -2$ ; B:  $\text{Rb}_{87}$ ,  $M = -1$ .

expected  $f(x_S)$  at those field values. The results are presented in Fig. 4. For  $x < 0$ , the agreement between calculated and measured detected atom distributions is somewhat poor. This side of the distribution is near the convex pole piece of the magnet, and the constant-force approximation made to derive Eq. (3) breaks down for atoms traveling too close to the pole piece. For  $x > 0$ , the agreement between calculated and measured  $f(x_S)$  is excellent. These results fully validate our experimental technique.

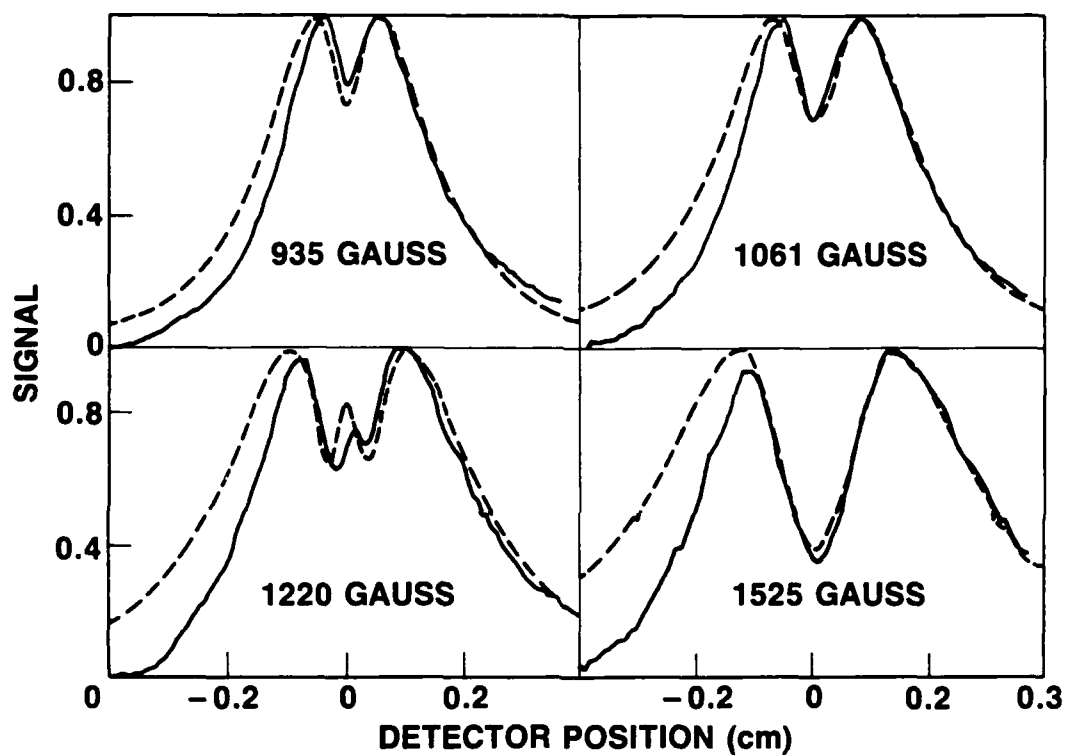


Fig. 4. Detected Rubidium Atom Distributions at Indicated Magnetic Fields. Oven temperature: 484 K. Solid line: measured distributions. Dashed line: calculated distributions for a Maxwellian beam.



## V. ATOMIC HYDROGEN VELOCITY DISTRIBUTIONS

Figure 5 reveals the atomic hydrogen beam fraction as a function of total pressure in the dissociator bulb, and discharge rf power. These data were obtained at a discharge frequency of 205 MHz. The discharge power was corrected for reflection, and the atomic fraction, measured with the quadrupole mass analyzer, was corrected for the  $H^+$  background when detecting  $H_2$ .

We have taken preliminary atomic hydrogen deflection data at total dissociator pressures of 0.2, 0.4, and 0.7 Torr, and at 995 and 1326 G magnetic fields. Zero-field-detected atom distributions have also been measured at each operating pressure. We then used Eq. (4) with the beam-Maxwellian distribution given by Eq. (7) to test the validity of the hypothesis of a thermal beam. The source temperature  $T$  was treated as a free parameter. Figure 6 exhibits, as an example, the deflection data at 995 G and 0.4 Torr, together with the expected detected atom distributions for Maxwellian beams at 300 and 500 K. As shown by Eq. (3), the transversal atomic displacement by the field is inversely proportional to  $V^2$ . Therefore, it is clear that the distribution at 300 K contains a large excess of slow atoms (large deflections), while the distribution at 500 K contains a correspondingly large excess of fast atoms (small deflections). Similar problems were encountered when analyzing the rest of the deflection data. These results indicate that the atomic velocity distribution in the beam must be significantly narrower than the beam-Maxwellian.

To estimate qualitatively the characteristics of the actual velocity distribution in our atomic hydrogen beam, we decided to model it by a Gaussian distribution of peak speed  $V_0$  and width parameter  $\sigma$ :

$$g(V) = \frac{1}{\sigma\sqrt{2\pi}} \exp [-(V - V_0)^2/2\sigma^2] \quad (8)$$

$V_0$  and  $\sigma$  were treated as free parameters and adjusted to provide a reasonable approximation to the measured deflection data. Given the preliminary nature

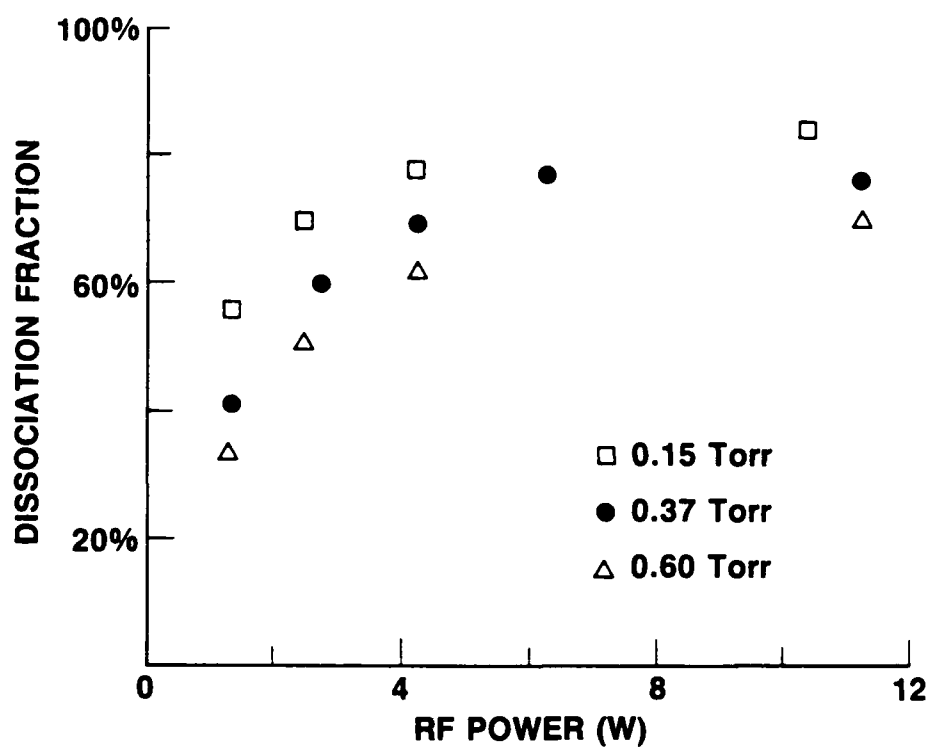


Fig. 5. Atomic Hydrogen Beam Fraction vs rf Discharge Power. Total dissociator bulb pressures are indicated.

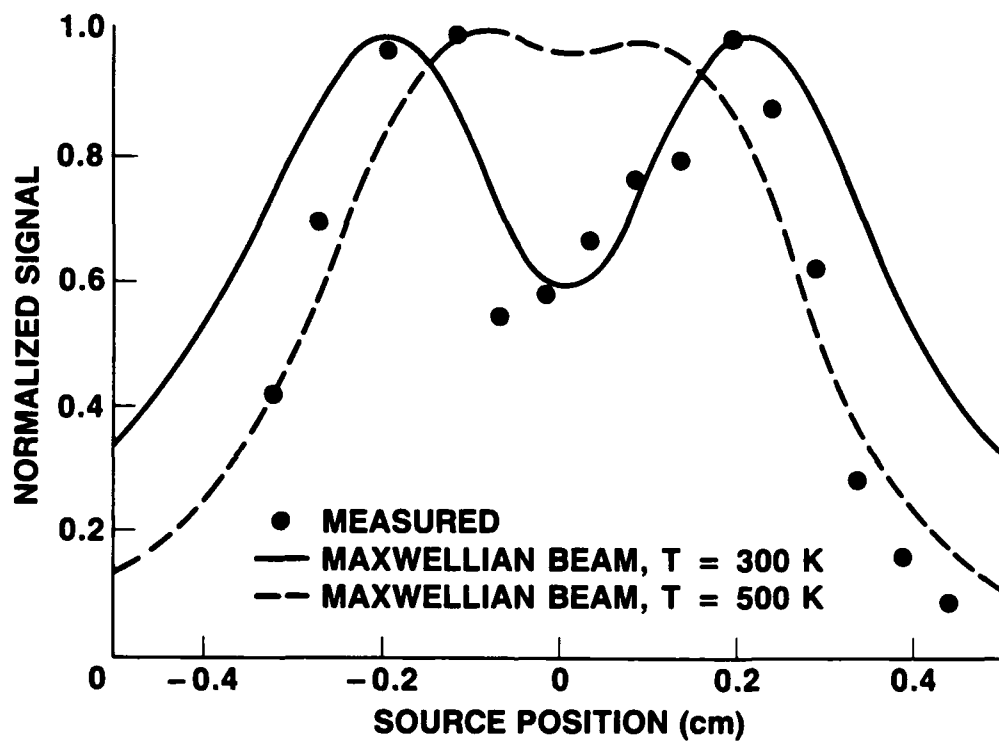


Fig. 6. Detected Hydrogen Atom Distribution at 995 G and 0.40 Torr. Dots: measured distribution. Curves: calculated distributions.

of the deflection data and model velocity distribution, no attempt was made to obtain a "best fit." Figures 7, 8, and 9 exhibit the deflection data at 995 G for dissociator total pressures of 0.2, 0.4, and 0.7 Torr, with the corresponding results calculated using the velocity distributions given by Eq. (8). A much closer agreement with the measured data is obtained than when using Maxwellians. Similar results were obtained for the data at 1326 G.

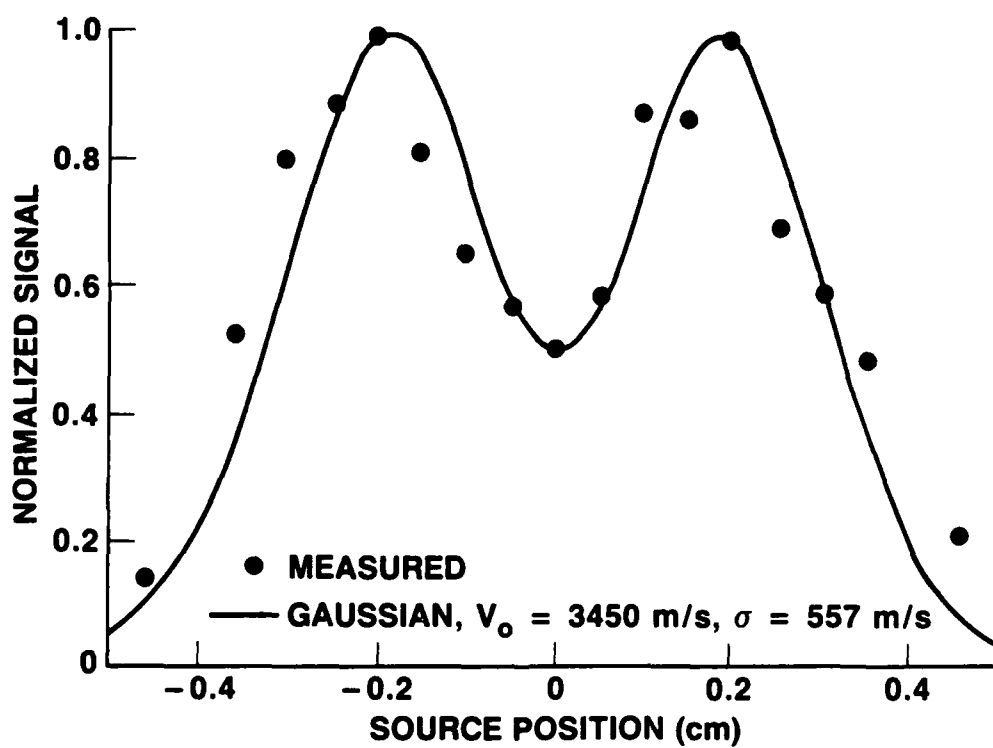


Fig. 7. Detected Hydrogen Atom Distribution at 995 G and 0.20 Torr. Dots: measured distribution. Curve: calculated distribution.

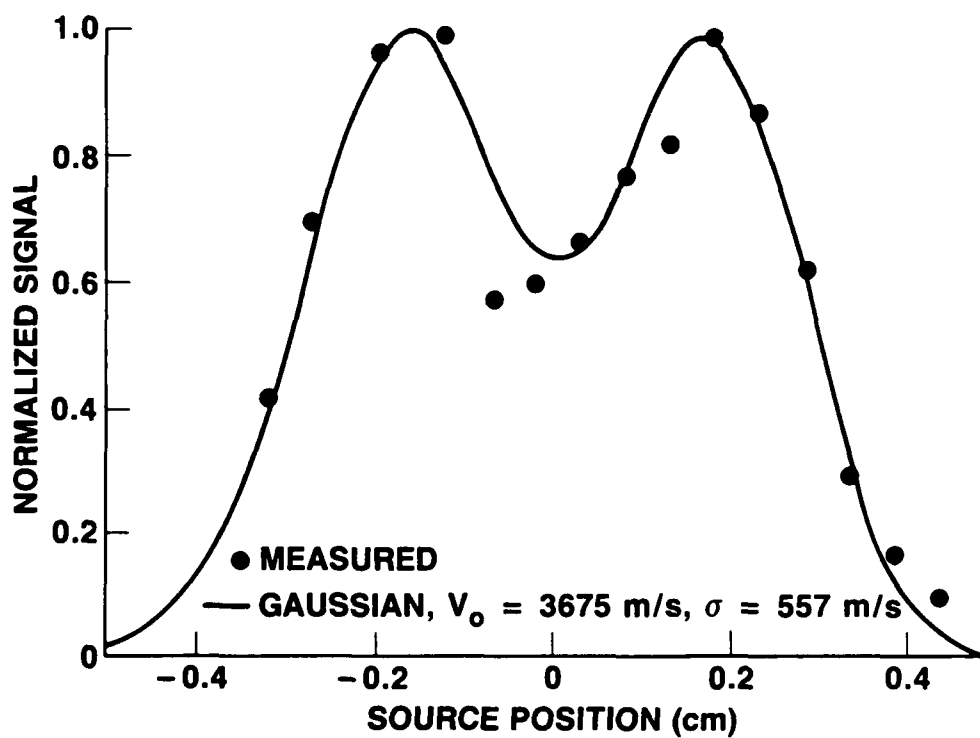


Fig. 8. Detected Hydrogen Atom Distribution at 995 G and 0.40 Torr. Dots: measured distribution. Curve: calculated distribution.

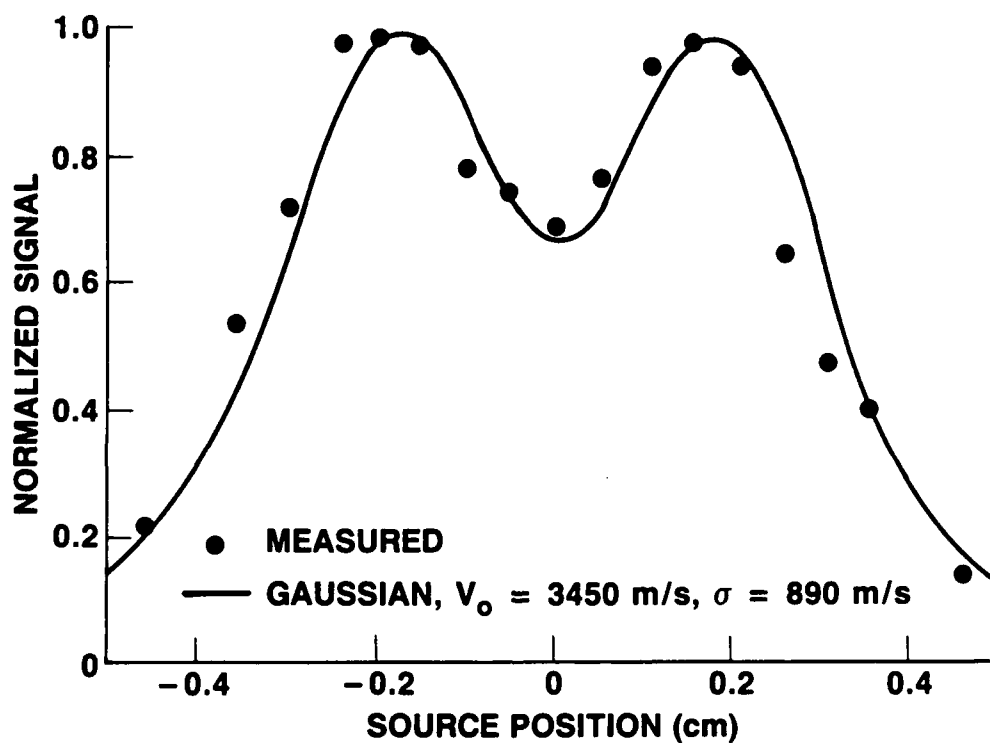


Fig. 9. Detected Hydrogen Atom Distribution at 995 G and 0.70 Torr. Dots: measured distribution. Curve: calculated distribution.

## VI. DISCUSSION AND CONCLUSIONS

The Gaussian velocity distributions used to calculate the results shown in Figs. 7-9 are presented in Figs. 10, 11, and 12, together with the corresponding Maxwellians having the same peak velocity. These figures reveal that the atomic beam velocity distributions are indeed nonthermal and much narrower than Maxwellians. Because the distribution at 0.7 Torr is broader than the distributions at 0.2 and 0.4 Torr, it is clear that we are not measuring distributions narrowed by gas-dynamics effects. Instead, incomplete thermalization of the hydrogen atoms must be the cause of the narrowing. This interpretation is consistent with the width of the distribution becoming close to the Maxwellian width as the discharge pressure increases.

The peak velocities correspond to kinetic energies of about 0.06 eV, much smaller than the approximately 2 eV of kinetic energy available per atom immediately after dissociation. Because the atoms must lose the excess energy without broadening significantly their energy distribution, the main energy-loss mechanism must be an inelastic process with a relatively large loss per collision. Vibrational excitation of the background hydrogen molecules (0.546 eV energy-loss/collision) seems to be a good candidate for such a process. Further studies in this area are required.

It is well known that the velocity passband of the hexapole or quadrupole magnets used as state selectors in hydrogen masers is rather narrow (about 25% full width at half maximum). Our findings indicate that it should be possible to design the state-selecting magnet having a velocity passband that matches as closely as possible the fairly narrow velocity distribution of the hydrogen atoms effusing out of the dissociator. Thus the efficiency with which the maser uses its hydrogen supply would be greatly enhanced.



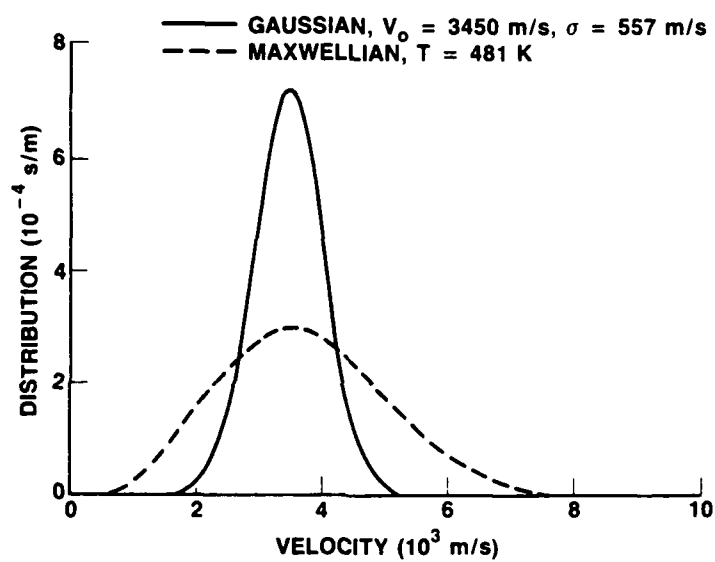


Fig. 10. Model Velocity Distributions Used for Fig. 7.

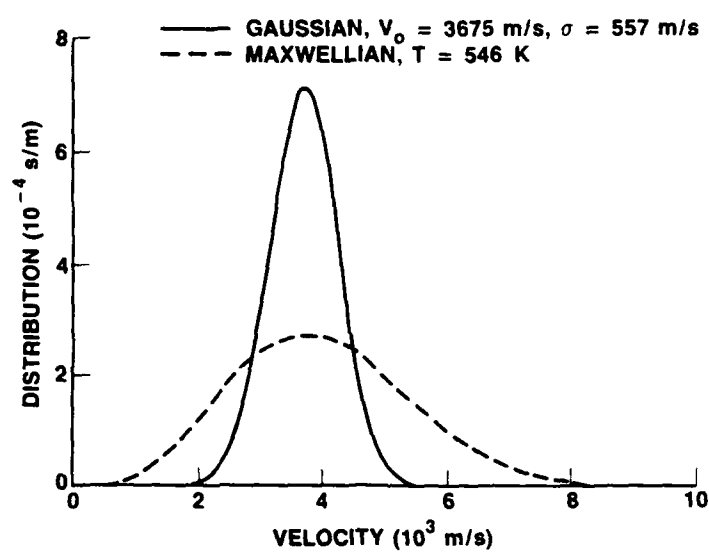


Fig. 11. Model Velocity Distributions Used for Fig. 8.

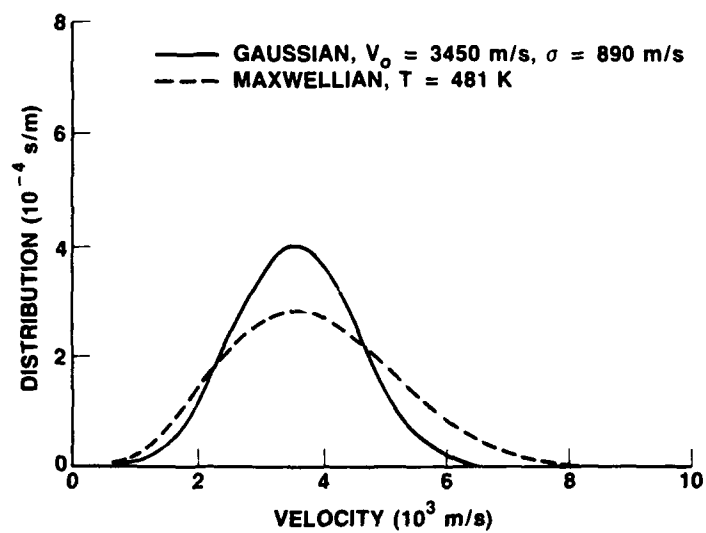


Fig. 12. Model Velocity Distributions Used for Fig. 9.

## REFERENCES

1. S. J. B. Corrigan and A. von Engel, "Excitation and Dissociation of Hydrogen by an Electron Swarm," Proc. Roy. Soc. A 245, 335 (1958).
2. J. T. M. Walraven and I. F. Silvera, "Helium-Temperature Beam Source of Atomic Hydrogen," Rev. Sci. Instrum. 53, 1167 (1982).
3. A. Hershcovitch, A. Kponou, and T. O. Niinikoski, "Cold High-Intensity Atomic Hydrogen Beam Source," Rev. Sci. Instrum. 58, 547 (1987).
4. T. M. Miller, "Atomic Beam Velocity Distributions with a Cooled Discharge Source," J. Appl. Phys. 45, 1713 (1973).
5. J. Viennet, P. Petit, and C. Audoin, "Régulateur de Débit d'Hydrogène à Réponse Rapide," J. Phys. E 6, 261 (1973).
6. I. I. Rabi, J. M. B. Kellogg, and J. R. Zacharias, "The Magnetic Moment of the Proton," Phys. Rev. 46, 157 (1934).
7. G. Breit and I. I. Rabi, "Measurement of Nuclear Spin," Phys. Rev. 38, 2082 (1931).
8. N. F. Ramsey, Molecular Beam, Oxford University Press, New York (1956), p. 400.
9. N. F. Ramsey, *ibid.*, p. 398.

## LABORATORY OPERATIONS

The Aerospace Corporation functions as an "architect-engineer" for national security projects, specializing in advanced military space systems. Providing research support, the corporation's Laboratory Operations conducts experimental and theoretical investigations that focus on the application of scientific and technical advances to such systems. Vital to the success of these investigations is the technical staff's wide-ranging expertise and its ability to stay current with new developments. This expertise is enhanced by a research program aimed at dealing with the many problems associated with rapidly evolving space systems. Contributing their capabilities to the research effort are these individual laboratories:

**Aerophysics Laboratory:** Launch vehicle and reentry fluid mechanics, heat transfer and flight dynamics; chemical and electric propulsion, propellant chemistry, chemical dynamics, environmental chemistry, trace detection; spacecraft structural mechanics, contamination, thermal and structural control; high temperature thermomechanics, gas kinetics and radiation; cw and pulsed chemical and excimer laser development, including chemical kinetics, spectroscopy, optical resonators, beam control, atmospheric propagation, laser effects and countermeasures.

**Chemistry and Physics Laboratory:** Atmospheric chemical reactions, atmospheric optics, light scattering, state-specific chemical reactions and radiative signatures of missile plumes, sensor out-of-field-of-view rejection, applied laser spectroscopy, laser chemistry, laser optoelectronics, solar cell physics, battery electrochemistry, space vacuum and radiation effects on materials, lubrication and surface phenomena, thermionic emission, photosensitive materials and detectors, atomic frequency standards, and environmental chemistry.

**Electronics Research Laboratory:** Microelectronics, solid-state device physics, compound semiconductors, radiation hardening; electro-optics, quantum electronics, solid-state lasers, optical propagation and communications; microwave semiconductor devices, microwave/millimeter wave measurements, diagnostics and radiometry, microwave/millimeter wave thermionic devices; atomic time and frequency standards; antennas, rf systems, electromagnetic propagation phenomena, space communication systems.

**Materials Sciences Laboratory:** Development of new materials: metals, alloys, ceramics, polymers and their composites, and new forms of carbon; nondestructive evaluation, component failure analysis and reliability; fracture mechanics and stress corrosion; analysis and evaluation of materials at cryogenic and elevated temperatures as well as in space and enemy-induced environments.

**Space Sciences Laboratory:** Magnetospheric, auroral and cosmic ray physics, wave-particle interactions, magnetospheric plasma waves; atmospheric and ionospheric physics, density and composition of the upper atmosphere, remote sensing using atmospheric radiation; solar physics, infrared astronomy, infrared signature analysis; effects of solar activity, magnetic storms and nuclear explosions on the earth's atmosphere, ionosphere and magnetosphere; effects of electromagnetic and particulate radiations on space systems; space instrumentation.